Elsevier Editorial System(tm) for Journal of Biomechanics

Manuscript Draft

Manuscript Number:

Title: Microstructure, Mineral and Mechanical Properties of Teleost Intermuscular Bones

Article Type: Full Length Article (max 3500 words)

Keywords: Teleost fish; intermuscular bone; mineral; mechanical properties

Corresponding Author: Dr. Jean Paul Berteau, Ph.D.

Corresponding Author's Institution:

First Author: Imke Fiedler

Order of Authors: Imke Fiedler; Baptiste Depalle; Andre Duarte; xizhe zhao; Luis Cardoso; Shi Jin; Jean-Philippe Paul Berteau, Ph.D.

Abstract: There is an increasing interest in understanding teleost bone biomechanics because of the current importance of teleosts as new biomedical models. Here, we have investigated the bone structure, Tissue Mineral Density (TMD), fracture profiles and micro-mechanical properties of 30 Intermuscular Bones of teleost fish - harvested from North Atlantic Herring of two age groups (young and old) - by using micro-computed tomography, wide-angle X-ray scattering, scanning electron microscopy and micro-mechanical tensile testing. Our study shows some astonishing properties of the Intermuscular Bones of the North Atlantic Herring : (i) young fish bones were 49 % higher in Young's modulus than old fish bones while their TMD was not statistically different and the crystal length was 8 % higher in the old fish bones, (ii) Intermuscular fish bones present higher ductility, lower Young's modulus but similar strength compared to literature of mammalian bones, and (iii) a parametric relationship has been depicted between the transition point (i.e. transition from the toe region to the linear-elastic region of the stress-strain curve) and the yield point for both strain and stress. Thus, our results revealed that Intermuscular Bones of teleost present a hybrid nature of soft and hard tissue that might be associated with their evolution from mineralized tendons. This study provides new data regarding teleost fish bone biomechanics and mineralization and describes a new relationship between toe region and linear-elastic region of these bone types.

Microstructure, Mineral and Mechanical Properties of Teleost Intermuscular Bones

Fiedler IAK[1], Depalle B[2], A. Duarte[1], Zhao X[3], Cardoso L[4], Jin S[3], Berteau JP*[1,5,6]

1 Department of Physical Therapy, City University of New York - College of Staten Island, USA;
2 Department of Materials, Imperial College London, UK;
3 Department of Chemistry, City University of New York – College of Staten Island, USA;
4 Department of Biomedical Engineering, City University of New York – City College of New York, USA;
5 New York Center for Biomedical Engineering, City University of New York – City College of New York, USA
6 Nanosciences Initiative, Advance Science Research Center, City University of New York, USA;

***Corresponding author:**
Jean-Philippe Berteau, PhD
Address: Department of Physical Therapy, School of Health Sciences at the College of Staten Island, 2800 Victory Boulevard, Staten Island, New York 10314, New York, USA.
Phone: (001) 718 982 2905
E-mail: Jean.Berteau@csi.cuny.edu

Abstract

There is an increasing interest in understanding teleost bone biomechanics because of the current importance of teleosts as new biomedical models. Here, we have investigated the bone structure, Tissue Mineral Density (TMD), fracture profiles and micro-mechanical properties of 30 Intermuscular Bones of teleost fish – harvested from *North Atlantic Herring* of two age groups (young and old) – by using micro-computed tomography, wide-angle X-ray scattering, scanning electron microscopy and micro-mechanical tensile testing. Our study shows some astonishing properties of the Intermuscular Bones of the *North Atlantic Herring* : (i) young fish bones were 49 % higher in Young's modulus than old fish bones while their TMD was not statistically different and the crystal length was 8 % higher in the old fish bones, (ii) Intermuscular fish bones present higher ductility, lower Young's modulus but similar strength compared to literature of mammalian bones, and (iii) a parametric relationship has been depicted between the transition point (*i.e.* transition from the toe region to the linear-elastic region of the stress-strain curve) and the yield point for both strain and stress. Thus, our results revealed that Intermuscular Bones of teleost present a hybrid nature of soft and hard tissue that might be associated with their evolution from mineralized tendons. This study provides new data regarding teleost fish bone biomechanics and mineralization and describes a new relationship between toe region and linear-elastic region of these bone types.

Keywords: Teleost fish; intermuscular bone; mineral; mechanical properties

1. Introduction

Bone tissue is a composite, porous and hierarchized biomaterial consisting of an organic soft matrix of collagen fibrils (tropocollagen – TC), an inorganic hard phase of mineral crystals (carbonated hydroxyapatite – cAp), several non-collagenous proteins, and water (Reznikov et al., 2014; Rho et al., 1998). To address the relationship between mineral-related parameters and bone mechanics, a strong body of evidence has depicted that poorly mineralized bone (start of the maturation) presents a weak and ductile mechanical behavior, and highly mineralized bone (end of the maturation) presents a strong and stiff mechanical behavior (Burstein et al., 1975; Currey, 1969, 1988; Currey et al., 1996; Donnelly et al., 2010a; Martin and Ishida, 1989). For instance, the increase of tissue mineral density (TMD) combined with a gradual increase in cAp size and stoichiometry has been linked to an increase in bending stiffness and failure moment (Donnelly et al., 2010b). However, this body of knowledge has been mainly depicted from studies investigating mammalian bone samples and because mammalian bone's hierarchized structure and porosity alter the failure mechanisms of bone, it remains challenging to establish a quantitative link between mineral-related parameters and alterations in mechanical properties of bone.

To overcome this challenge in continuum mechanics, one specific bone type within the skeleton of teleost fish, i.e. Intermuscular Bones (IBs), present some interesting features including a simple structural hierarchy and well-aligned fiber and crystal orientation along the whole bone (Burger et al., 2008; Lee and Glimcher, 1991; Rho et al., 2001). One major advantage of these features is that IBs from fish could be assumed to be more homogeneous, isotropic and continuous than bone samples from mammalians. However, while these structural features generate a recently increasing interest in teleost bones for deciphering the relationship between biological components and mechanics of mineralized tissues, biological and mechanical data of teleost intermuscular bones remain scarce in the scientific literature.

In this study we have used one teleost – the *North Atlantic Herring* – to investigate the biomechanics of intermuscular bone at the microscale. We have hypothesized that IBs of *North Atlantic Herring* (i) show a lower tissue mineral density and a smaller crystal size in immature compared to mature stage, and (ii) show a weak and ductile mechanical behavior in immature stage and a strong and stiff mechanical behavior in mature stage. To test our hypotheses, IB of two tissue ages were investigated to obtain their mechanical properties and profile of fracture, their bone mineral density, porosity and bone structure at the micro-scale, and their crystal size (s. Figure 1).

2. Material and methods

2.1 Animal model

IBs were extracted from a total of four *Atlantic Herring* fish, acquired fresh from a local fish market. Each bone sample was wrapped in gauze soaked with phosphate buffered saline (PBS) and Protease Inhibitor (PI), and stored at -20 °C. Samples presented a rod-like shape and an ellipsoidal cross-section with a diameter of less than 200 μm, and were assigned to two groups according to the body length of the fish (juvenile fish < 25 cm < adult fish (O'Brian et al., 1990); young bone, N=9; old bone, N=21).

2.2 Micro-mechanical tensile testing

Mechanical testing was performed using a micro-tester (Xpert4000, ADMET, Norwood, MA, USA) customized with serrated pinching grips covered with carbide sand paper (P500) to prevent samples from slipping. Samples were positioned vertically with an initial gauge length of 3.0 mm and approximately 3.5 mm of both extremities being clamped. Samples were kept hydrated during the tests with PBS. Uniaxial tensile loading – displacement control with a speed of 10 µm/s corresponding to a quasi-static engineering strain rate (Wright and Hayes, 1976) – was applied while force was measured with a load cell (100 N) and displacements were recorded in terms of change in actuator position. Conversions from force and displacement to engineering stress and engineering strain according to Hooke's law for isotropic materials were performed with a custom-written Matlab script (MATLAB 2016b, Mathworks, MA, USA). Several parameters were derived as depicted in Figure 2 A. The toe region (region I - assessed from the beginning of the curve to the transition point, *i.e.* onset of the linear region of the curve) was used to determine the transition stress (σ_t) and transition strain (ε_t) (Herbert et al., 2016). The yield point (ε_y, σ_y) was determined using the 0.2% offset method, and used to separate the elastic region (region II - measured from the transition point to the yield point) and the plastic region (region III - measured from the yield point to the fracture point ($\varepsilon_{max,}$ σ_{max}). Young's modulus was determined as the slope of the curve within the linear displacement region, and the work-until-fracture, *i.e.* total work, was determined by calculating the area under stress-strain curve. Elastic and plastic work were determined by calculating the area under the curve in region II and III, respectively. The uncertainty of measurement for stress and strain was determined to be 3.9 % and <0.1 %, respectively. Machine compliance was measured by means of reproducibility and accuracy tests on samples of known materials (wood, polystyrene, nylon) with similar diameters as the IB samples.

2.3 Scanning electron microscopy (SEM)

SEM was performed to visualize fracture profiles and to examine the topography of fracture surfaces (N=3 per group). Samples were carefully onto SEM stubs using carbon tape. Imaging was performed using a scanning electron microscope (Helios NanoLab, DualBeam, FEI, Hillsboro, Oregon, USA) with an Everhart-Thornley detector in secondary electron mode (beam voltage of 2 kV and current of 25 pA).

2.4 High resolution micro-computed tomography scanning (HR-μCT)

On both tissue age groups (young: N=3, old: N=5), tissue mineral density (TMD) was determined using HR-μCT (SkyScan 1172, Bruker, Kontich, BE) at a voxel size of 4 μm, X-ray energy of 100 keV and intensity of 100 μA. The region of interest corresponded to the initial gauge length of mechanically tested samples. Water, air and hydroxyapatite phantoms (0.25 gHA/cm^3 and 0.75 gHA/cm^3) were used for calibration and a custom-written Matlab code was used to determine the average TMD per sample.

2.5 Wide-angle X-ray scattering

Fish bone samples from both tissue age groups (young: N=3, old: N=5) were investigated using a laboratory WAXS machine (NanoSTAR, Bruker AXS, Billerica, MA, USA) with a CuKα X-ray source (wavelength of 0.154 nm and beam size of approximately 1 mm). The region of interest for each sample was defined centrally within the initial gauge length of samples that previously underwent micro-tensile testing. Acquisition time was 6 hours and beam center calibration was performed using silicon reference powder. Resulting 2D WAXS patterns were processed according to commonly used methods (Pabisch et al., 2013). Crystal length, corresponding to the length along the (002) crystal lattice axis (*i.e.* long axis of cAp) was determined with the Scherrer equation (1), where L represents the crystal length, K a shape factor dedicated to crystal lattice structure ($0.9 < K < 2.0$), λ the X-ray wavelength, B the full width at half maximum of the Bragg' diffraction peak in radians, and Θ half of the respective diffraction angle. Within this study, $K = 0.9$ has been used.

$$L = K \lambda / (B \Theta) \qquad (1)$$

2.6 Statistical analysis

Statistical analyses were performed using SPSS (IBM SPSS Statistics, Version 20.0, Armonk, NY, USA). Normality and homoscedasticity of all data were tested with Shapiro-Wilk's and Levene's tests, respectively. In case of normal distribution and equal variance, parametric tests were used. Otherwise, non-parametric tests were performed. Parametric comparisons of mechanical properties were made with an independent t-test and non-parametric comparisons of TMD and cAp length were made with the Mann-Whitney-U test. Linear relationships were assessed with Pearson. All tests were performed at a significance level of $\alpha = 0.05$.

3. Results

Mechanical characterization of IBs using micro-mechanical tensile testing showed that IB undergo a distinct transition from a toe region to a linear-elastic region and a distinct yield point from a linear-elastic region to a plastic region in samples independent of age group. Furthermore, significant differences between the two investigated age groups with regard to their elastic behavior were found. The extracted mechanical properties and cross-sectional areas are listed in Table 1.

Regarding the transitional behavior of IB specimens, *i.e.* the pooled data of both age groups, a statistical relationship was found between the toe region and the elastic region showing a significant Pearson correlation between transition strain and yield strain with $p<0.001$ and

R^2=0.82 as shown in Figure 2 B, and between transition stress and yield stress with $p<0.001$ and R^2=0.30 as shown in Figure 2 C. On average, the total strain range was composed of 8 % strain exhibited within the toe region, 10 % strain exhibited within the elastic region, and 82 % strain exhibited within the plastic region.

When comparing the mechanical properties of the two age groups, no significant differences were found regarding the transition point from toe to linear-elastic region. Regarding the elastic behavior, Young's modulus was significantly higher in young bones with 4.3 (±1.1) GPa than old bone with 2.6 (±0.5) GPa ($p = 0.002$, independent t-test), resulting in a difference of 49 %. While yield stress was similar between the groups, yield strain was significantly lower in young specimens compared to old specimens with 0.027 (±0.008) vs. 0.036 (±0.008), $p=0.008$). Maximum stress was similar between the groups with 121.9 (±34.3) MPa in young and 107.5 (±22.6) MPa in old tissue, and maximum strain showed a trend towards lower values in young tissue with 0.18 (±0.5) compared to older tissue with 0.22 (±0.1). The mean total work was similar between groups with 17.3 (±8.2) MPa in young and 19.2 (±8.7) MPa in old tissue. Elastic and plastic work were similar in both groups. Representative stress-strain curves and fracture profiles of the young and old group are shown in the SEM images in Figure 3 A and B. In both groups, profiles presented fracture surfaces indicative of brittle fracture behavior, *i.e.* cross-sectional fractures, while higher magnification further exposed vertical collagen fiber delamination.

A 3D µCT reconstruction of a whole IB specimen including the investigated region of interest is shown in Figure 4 A. Structural characterization with µCT showed that IBs did not present porous structures at the scale of investigation (Figure 4 B). As depicted in Figure 4 C, both young and old bone tissue showed homogeneous mineralization both transversally and longitudinally. With regard to TMD at the microscale, no significant differences were detected between the groups - both groups yielded a TMD of 1.6 (±0.1) gHAP/cm^3. We found a smaller crystal length L in young bones with 12.1 (±0.46) nm than in old bones with 13.1 (±0.45) nm, yielding a small but significant difference of 8 % (p=0.025, Mann-Whitney U test), see Table 1.

4. Discussion

In this study, we investigated the Intermuscular Bones (IBs) of the *North Atlantic Herring* with regard to its structure and organization at the micro-scale, its mineral-related properties, and its micro-mechanical tensile properties. Our results show that these IBs present no porous micro-structures and a homogenous mineral distribution along their long axis. Furthermore, our results show that these IBs feature special mechanical characteristics of both soft tissue (*e.g.* tendon) and hard tissue (*e.g.* mammalian cortical bone). Additionally, our results show that the microscopic degree of mineralization was independent of the age group of the fish while a higher crystal length and a lower Young's modulus was displayed in the older IBs.

Our 3D μCT images showed that IBs have a cylindrical, long and thin fiber-like geometrical shape at the whole bone level, and revealed that they do not present micro-porosity, osteon-like structures or lamellae at the microscale for both investigated tissue ages. Thus, our μCT imaging results support the presence of a simplified structure in IB compared to mammalian bone which is composed of up to nine hierarchical levels (Reznikov et al., 2014). The degree of mineralization at the microscale was homogenous along the long axis and the crystal length (L) was with < 15 nm for both age groups below reported crystal length of mammalian bone (Acerbo et al., 2014). While crystals in mammalian bone are suggested to grow from within the gap and overlap regions of collagen fibrils (67 nm periodicity) (Balooch et al., 2008; Nair et al., 2014) into the extra-fibrillar space where they can likely reach larger dimensions, the detected crystal size in IB remains below the length of extra-fibrillar crystals, supporting previous studies suggesting sole intra-fibrillar mineral deposition in IBs (Lee and Glimcher, 1991). Furthermore, we prepared one ultra-thin lamellae of one IB sample of an adult fish using focused ion beam etching, and performed transmission electron microscopy (see supplemental Figure S1). Imaging supports that IB tissue is built of longitudinally aligned collagen, depicting the typical periodicity of collagen fibers with highly aligned inorganic crystals deposited within the tissue, measuring up to 4 nm in thickness.

Regarding their mechanical properties, our results show IBs with an astonishing combination of mechanical characteristics of both soft (*e.g.* tendon) and hard (*e.g.* mammalian cortical bone) tissues. Specifically, IBs presented some soft tissue characteristics including: (i) a distinct toe region prior to entering linear elastic deformation, (ii) a Young's modulus of one order of magnitude lower than mammalian cortical bone, and (iii) a pronounced plastic deformation regime. Meanwhile, IBs presented some hard tissue characteristics including similar strength – measured by means of the maximum stress – to those usually found in mammalian cortical bone (Carter and Spengler, 1978; Cowin, 1985; Li et al., 2013; Mirzaali et al., 2016). However, IBs work-to-fracture values depicted a larger ability for post-yield deformation compared to mammalian bones while hosting a considerable amount of mineral within the fibrils (*i.e.* TMD in the range of mammalian bone). Indeed, IBs fracture strains reached up to 22 % which is much higher than mammalian cortical bone which elongates only by a few percent (Liu et al., 2014), or tendons with maximum strains reported around 10 % (Matson et al., 2012). IBs further expressed a pronounced post-yield deformation behavior (80 % of total strain) during the plastic deformation regime (region III in the stress-strain curve) and presented a low Young's modulus in the magnitude of light, non-mineralized tendons (Bennett et al., 1986; Matson et al., 2012). Interestingly, significant parametric correlations have been found between the transition point (exit point of the toe region) and the yield point which shows that stress and strain at the transition point are linked to stress and strain at the yield point, respectively. Indeed, the variance of the transition point strain explains 82% of the variance of the yield strain, and the variance of the transition point stress explains 30% of the variance of the yield stress. Based on these observations, we suggest that IBs from AH belong to a group of composite tissues presenting a particular combination of properties from soft and hard tissues, possibly governed by its microstructural organization which is derived from tendons within the musculoskeletal system of the teleost (Yao et al., 2015). To summarize, our study presents a biomaterial with a rare combination of stiffness, strength and toughness, and a new quantitative link between its transition and yield point data.

Regarding the comparison between two stages of tissue age, differences were found both in Young's modulus at the microscale and in crystal length at the nanoscale, but not in the degree of mineralization at the microscale. Specifically, we found a significant 8 % smaller crystal size in young IB tissue compared to older tissue, supporting an increase in crystallinity and crystal size during the bone aging (Jäger and Fratzl, 2000; Nair et al., 2013; Vercher-Martinez et al., 2015; Ziv and Weiner, 2009). Regarding the mechanical properties of IBs during aging, a significantly lower Young's modulus has been detected in old compared to young IB tissue which contradicts our initial hypothesis and the theoretical optimization hypothesis (Wang et al., 2012). The scenario of lower stiffness at larger mineral length could be related to the degradation of the other biological components in the collagen matrix. For instance, the suggested lack of remodeling in this tissue might lead to a degradation of mechanical properties in IB through the accumulation of micro-cracks or nano-porous structures. An in-depth analysis of the composition and interconnectivity of the collagen in IBs could help reveal the specific failure mechanisms in this type of mineralized tissue. While an explanation for the nano-structural and molecular origin of the special mechanical behavior of IBs was not in the scope of this study, we propose IBs as an interesting tissue to study the complex interplay between a collagenous soft phase and a reinforced hard mineral phase in biomaterials.

5. Conclusion

This study shows that Intermuscular Bones of the *North Atlantic Herring* show a unique combination of stiffness, strength and toughness where a new quantitative link between their transition and yield point data has been depicted. Additionally, the microscopic degree of mineralization of IB is independent of the age of the fish while an increase in crystal size and a decrease in Young's modulus was displayed in the more mature Intermuscular Bones. Furthermore, our results show that these IBs feature special mechanical characteristics of both soft tissue (*e.g.* tendon) and hard tissue (*e.g.* mammalian cortical bone).

Acknowledgements: This work was supported by the National Science Foundation (CMMI-1333560 and MRI-1229449) and the National Institutes of Health (DK103362) (L.C.), Wellcome Trust grant WT097347MA (B.D.), PSC CUNY grant 68853-0046, CSI Provost's grant and CSI Start Up Funds (J.P.B.). The authors wish to thank Chaim M. Zieg for his extended assistance in acquiring fresh Atlantic herring fish samples.

Conflict of Interest: The authors declare that they have no conflict of interest.

References

Acerbo, A.S., Kwaczala, A.T., Yang, L., Judex, S., Miller, L.M., 2014. Alterations in collagen and mineral nanostructure observed in osteoporosis and pharmaceutical treatments using simultaneous small- and wide-angle X-ray scattering. Calcified Tissue International 95, 446–456.

Balooch, M., Habelitz, S., Kinney, J.H., Marshall, S.J., Marshall, G.W., 2008. Mechanical properties of mineralized collagen fibrils as influenced by demineralization. Journal of Structural Biology 162, 404–410.

Bennett, M.B., Ker1, R.F., Imery, N.J., Alexander, R.M., 1986. Mechanical properties of various mammalian tendons. Journal of Zoology 209, 537–548.

Burger, C., Zhou, H.-w., Sicŝ, I., Hsiao, B.S., Chu, B., Graham, L., Glimcher, M.J., 2008. Small-angle X-ray scattering study of intramuscular fish bone: collagen fibril superstructure determined from equidistant meridional reflections. Journal of Applied Crystallography 41, 252–261.

Burstein, A.H., Zika, J.M., Heiple, K.G., Klein, L., 1975. Contribution of collagen and mineral to the elastic-plastic properties of bone. The Journal of Bone & Joint Surgery 57, 956–961.

Carter D.R. and Spengler D.M., Mechanical properties and composition of cortical bone, Clinical Orthopedics and Related Research (135) (1978) 192–217.

Cowin S.C., 1983. The mechanical and stress adaptive properties of bone. Annals of Biomedical Engineering 11(3-4), 263-95.

Currey, J.D., 1969. The relationship between the stiffness and the mineral content of bone. Journal of Biomechanics 2, 477–480.

Currey, J.D., 1988. The effect of porosity and mineral content on the Young's modulus of elasticity of compact bone. Journal of Biomechanics 21, 131–139.

Currey, J.D., Brear, K., Zioupos, P., 1996. The effects of ageing and changes in mineral content in degrading the toughness of human femora. Journal of Biomechanics 29, 257–260.

Donnelly, E., Boskey, A.L., Baker, S.P., van der Meulen, M.C.H., 2010a. Effects of tissue age on bone tissue material composition and nanomechanical properties in the rat cortex. Journal of biomedical materials research. Part A 92, 1048–1056.

Donnelly, E., Chen, D.X., Boskey, A.L., Baker, S.P., van der Meulen, M.C.H., 2010b. Contribution of mineral to bone structural behavior and tissue mechanical properties. Calcified Tissue International 87, 450–460.

Herbert, A., Brown, C., Rooney, P., Kearney, J., Ingham, E., Fisher, J., 2016. Bi-linear mechanical property determination of acellular human patellar tendon grafts for use in anterior cruciate ligament replacement. Journal of Biomechanics 49, 1607–1612.

Jäger, I., Fratzl, P., 2000. Mineralized Collagen Fibrils. A Mechanical Model with a Staggered Arrangement of Mineral Particles. Biophysical journal 79, 1737–1746.

Lee, D.D., Glimcher, M.J., 1991. Three-dimensional spatial relationship between the collagen fibrils and the inorganic calcium phosphate crystals of pickerel (Americanus americanus) and herring (Clupea harengus) bone. Journal of Molecular Biology 217, 487–501.

Li S., Demirci E., Silberschmidt V.V., 2013. Variability and anisotropy of mechanical behavior of cortical bone in tension and compression. Journal of the Mechanical Behavior of Biomedical Materials 21, 109-20.

Liu, Y., Thomopoulos, S., Chen, C., Birman, V., Buehler, M.J., Genin, G.M., 2014. Modelling the mechanics of partially mineralized collagen fibrils, fibres and tissue. Journal of the Royal Society, Interface / the Royal Society 11, 20130835.

Martin, R.B., Ishida, J., 1989. The relative effects of collagen fiber orientation, porosity, density, and mineralization on bone strength. Journal of biomechanics 22, 419–426.

Mirzaali M.J., Schwiedrzik J.J., Thaiwichai S., Best J.P., Michler J., Zysset P.K., Wolfram U., 2016. Mechanical properties of cortical bone and their relationships with age, gender, composition and microindentation properties in the elderly. Bone 93, 196-211.

Matson, A., Konow, N., Miller, S., Konow, P.P., Roberts, T.J., 2012. Tendon material properties vary and are interdependent among turkey hindlimb muscles. The Journal of experimental biology 215, 3552–3558.

Nair, A.K., Gautieri, A., Buehler, M.J., 2014. Role of Intrafibrillar Collagen Mineralization in Defining the Compressive Properties of Nascent Bone. Biomacromolecules, 140623144155007.

Nair, A.K., Gautieri, A., Chang, S.-W., Buehler, M.J., 2013. Molecular mechanics of mineralized collagen fibrils in bone. Nature Communications 4, 1724.

O'Brian L., Burnett J., Mayo R.K., 1990. Maturation of Nineteen Species of Finfish off the Northeast Coast of the United States, 195.

Pabisch S., Wagermaier W., Zander T., Li C., Fratzl P., 2013. Imaging the nanostructure of bone and dentin through small- and wide-angle X-ray scattering, Methods in enzymology 532, 391–413.

Reznikov, N., Shahar, R., Weiner, S., 2014. Bone hierarchical structure in three dimensions. Acta Biomaterialia 10, 3815–3826.

Rho, J.Y., Mishra, S.R., Chung, K., Bai, J., Pharr, G.M., 2001. Relationship between ultrastructure and the nanoindentation properties of intramuscular herring bones. Annals of biomedical engineering 29, 1082–1088.

Rho, J.-Y., Kuhn-Spearing, L., Zioupos, P., 1998. Mechanical properties and the hierarchical structure of bone. Medical Engineering & Physics 20, 92–102.

Vercher-Martinez, A., Giner, E., Arango, C., Fuenmayor, F.J., 2015. Influence of the mineral staggering on the elastic properties of the mineralized collagen fibril in lamellar bone. Journal of the Mechanical Behavior of Biomedical Materials 42, 243–256.

Wang, Y., Azaïs, T., Robin, M., Vallée, A., Catania, C., Legriel, P., Pehau-Arnaudet, G., Babonneau, F., Giraud-Guille, M.-M., Nassif, N., 2012. The predominant role of collagen in the nucleation, growth, structure and orientation of bone apatite. Nature Materials 11, 724–733.

Wright T.M., Hayes W.C., 1976. Tensile testing of bone over a wide range of strain rates: effects of strain rate, microstructure and density. Journal of Medical and Biological Engineering 14 (6), 671–680.

Yao, W., Lv, Y., Gong, X., Wu, J., Bao, B., 2015. Different ossification patterns of intermuscular bones in fish with different swimming modes. Biology open 4, 1727–1732.

Zhang, D., Wu, X., Chen, J., Lin, K., 2018. The development of collagen based composite scaffolds for bone regeneration. Bioactive materials 3, 129–138.

Ziv, V., Weiner, S., 2009. Bone Crystal Sizes: A Comparison of Transmission Electron Microscopic and X-Ray Diffraction Line Width Broadening Techniques. Connective Tissue Research 30, 165–175.

Figure Captions

Figure 1 Experimental set-up of multimodal analysis. Intermuscular bone (IB) from juvenile and adult fish were assigned to two tissue age groups (young vs. old) to investigate the mechanical properties, micro-structure and mineral-related parameters.

Figure 2 Mechanical characteristics of intermuscular bone. **(A)** Exemplary engineering stress-strain curve of IB tested in tension, showing a toe region I from the beginning of the curve until reaching a transition point (σ_t ,ε_t), a linear-elastic region II until reaching the yield point (σ_y,ε_y) and a plastic region III until reaching a failure point (σ_{max},ε_{max}). The total amount of strain experienced in the toe region was similar to the amount of strain in the linear-elastic region, contributing 8 % and 10 % to the total maximum strain, respectively. The strain IBs experienced in region III contributed to the total strain by more than 80%, indicating that IB have a large capacity for plastic deformation before they undergo failure, yet they undergo a distinct fracture. Significant correlations were found between **(B)** the transition strain and yield strain (Pearson correlation, R^2=0.82, $p<0.001$), and **(C)** between transition stress and yield stress (Pearson correlation, R^2=0.30, $p=0.005$) showing that deformations in these two regions are proportional.

Figure 3 Mechanical properties of young and old Intermuscular Bones. **(A)** Engineering stress-strain curves of representative samples from different tissue ages, where young tissue showed significantly higher Young‘s modulus than older bones. **(B)** SEM micrographs from mechanically tested young and old bone tissue samples display signs of brittle fractures with clear transversal fractures in both groups, as well as ruptured, fibrous structures and fiber delamination at high magnification.

Figure 4 Microscopic structure and mineral density of Intermuscular Bone (IB) assessed with micro-CT at a voxel size of 4 µm. **(A)** 3D reconstruction of an IB specimen with the volume of interest (VOI) investigated within this study. **(B)** Cross-sectional view of young and old IB shows ellipsoidal geometry without the presence of porous structures. **(C)** Tissue mineral density (TMD) plotted along the long axis of the VOI (left graph, black line corresponds to mean value within a slice, gray lines correspond to the standard deviation within a slice) and TMD plotted across a transversal section. At both ages and in both directions, mineralization appears homogenously distributed.

Table captions

Table 1

Results of multimodal experimental analysis of intramuscular bone (IB) of Atlantic herring from young and old age presented in mean (± standard deviation). Significantly different parameters with a significance level of 0.05 are indicated with an asterisk.

Supplemental Data

Figure S1 caption

Structural information on collagen alignment and crystal morphology in IB: Transmission electron microscopy applied on longitudinal sections of the IB specimen allowed to display the uniaxial (horizontal) collagen fiber alignment along the long axis of one exemplary IB specimen with typical collagen periodicity (67 nm). TEM imaging within the IB allowed to visualize the distribution of mineral crystals within these regions (dark, long and thin structures at highest magnification) supporting the assumption that IBs feature a simplistic microstructure compared to hierarchical mammalian bone. IB provides an interesting soft-hard tissue hybrid biomaterial with simplified submicron architecture and specific mechanical properties.

Figure
Click here to download high resolution image

Figure 1

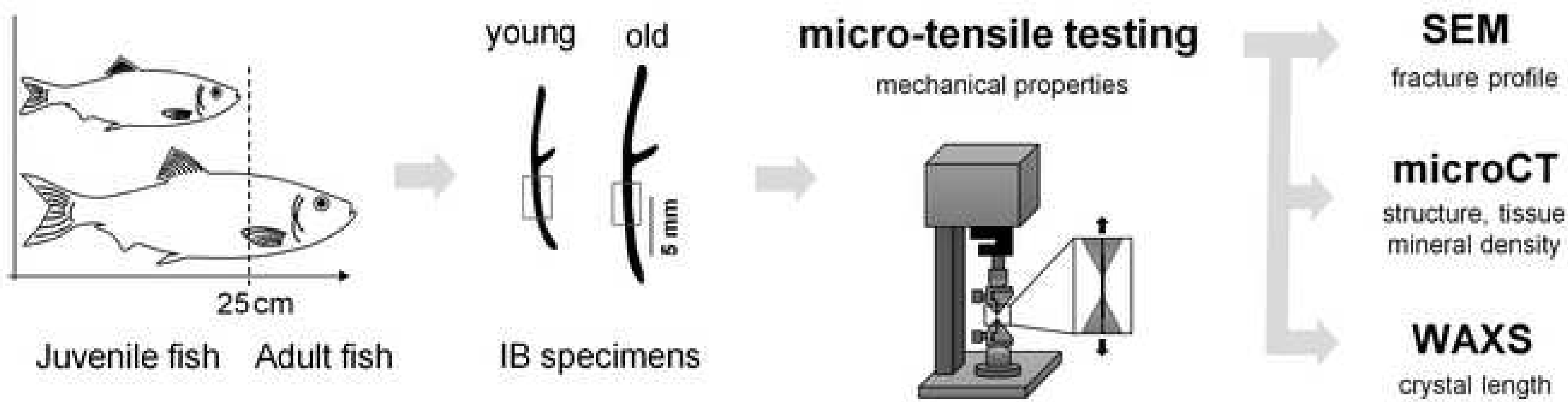

Figure
Click here to download high resolution image

Figure 2

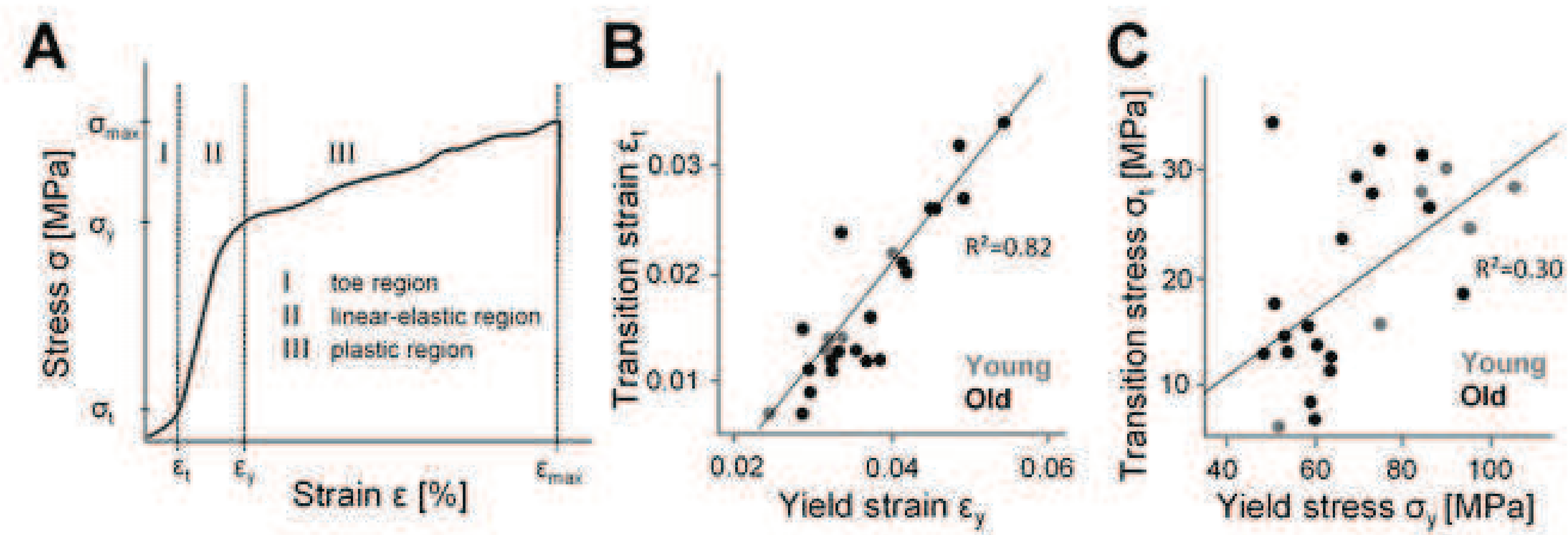

Figure
Click here to download high resolution image

Figure 3

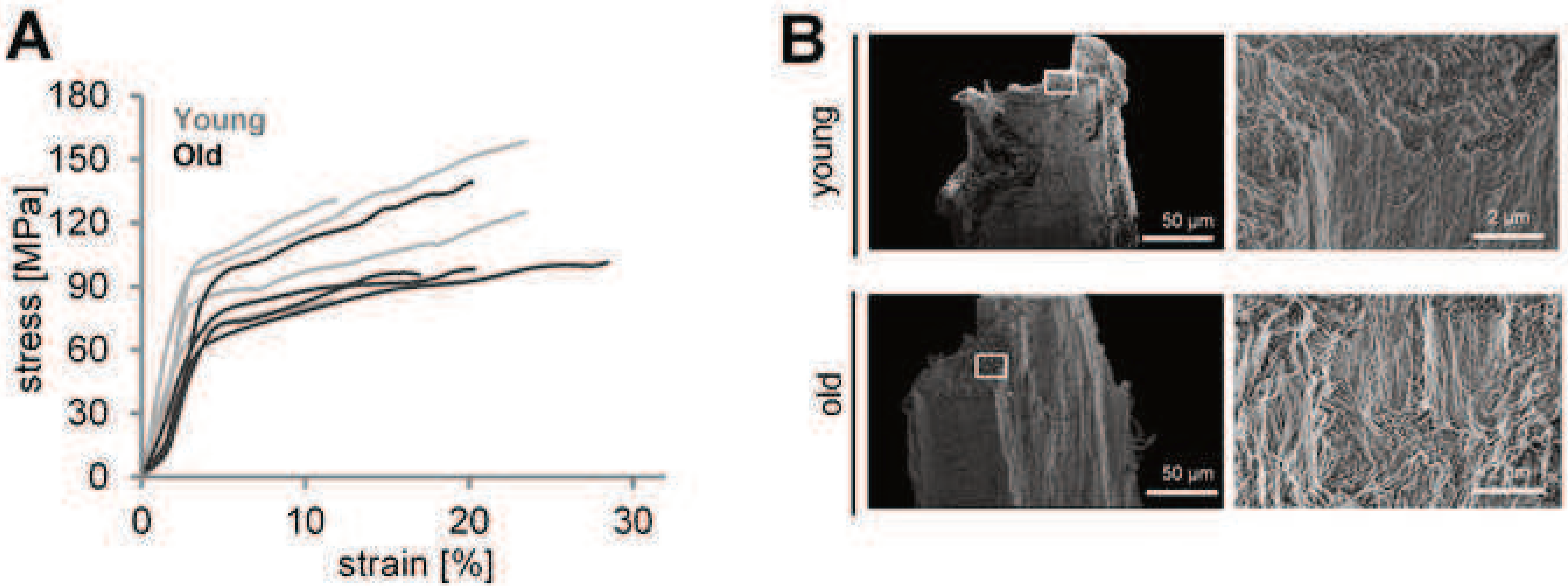

Figure

Click here to download high resolution image

Figure 4

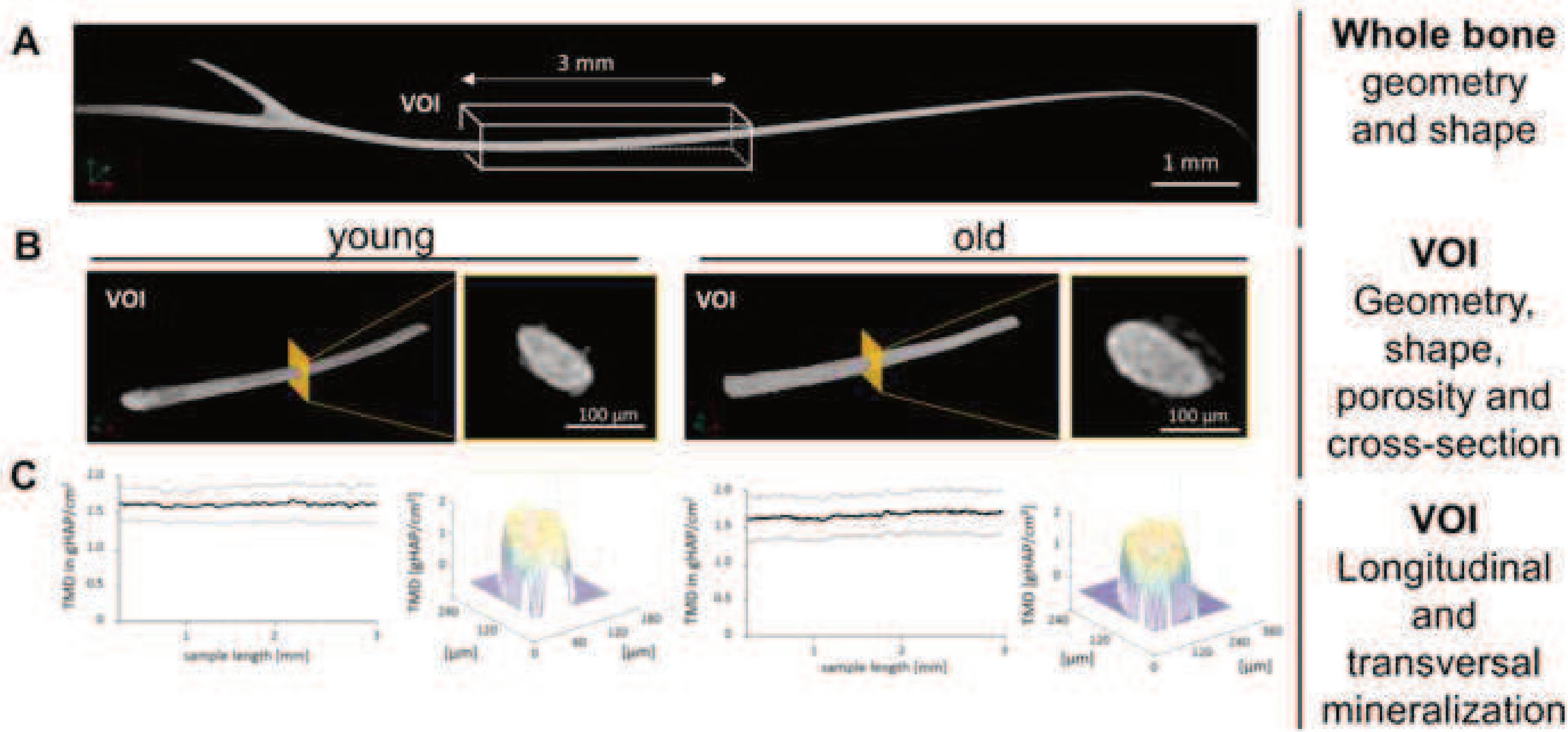

Table

Table 1

	Young IB		Old IB		
Transition strain (-)	0.014	(±.005)	0.018	(±0.008)	
Transition stress (MPa)	21.1	(±10.0)	18.8	(±9.1)	
Yield strain (-)*	0.027	(±0.008)	0.036	(±0.008)	*p=0.008
Yield stress (MPa)	72	(±22)	63	(±13)	
Young's modulus E (GPa)*	4.3	(±1.1)	2.6	(±0.5)	*p=0.002
maximum stress (MPa)	122	(±34)	108	(±22)	
maximum strain (-)	0.18	(±0.5)	0.22	(±0.08)	
toe work (MPa) (-)	0.091	(±0.067)	0.111	(±0.100)	
elastic work (MPa)	0.8	(±0.4)	0.9	(±0.3)	
plastic work (MPa)	16.5	(±8.0)	18.3	(±8.6)	
total work (MPa)	17.3	(±8.2)	19.2	(±8.7)	
Cross-sectional area (mm^2)*	0.04	(±0.01)	0.09	(±0.02)	*p<0.001
Crystal length L (nm)*	12.1	(±0.46)	13.1	(±0.45)	*p=0.025
Tissue Mineral Density (gHAP/cm^3)	1.6	(±0.1)	1.6	(±0.1)	

Supplementary Material

Click here to download Supplementary Material: Figure_S1_final.TIF

***Conflict of Interest Statement**

Conflict of Interest

Authors have no conflict of interest to disclose